Title

Structural Understanding of Self-Assembled Rare Earth Disilicide Nanostructures Via Scanning Probe Microscopy and First Principles Studies

Journal

Israel Journal of Chemistry, 48(2)

ISSN

0021-2148

Authors

Shinde, Aniketa

Cao, Juexian

Wu, Ruqian

et al.

Publication Date

2008-10-01

DOI

10.1560/ijc.48.2.73

Structural Understanding of Self-Assembled Rare Earth Disilicide Nanostructures Via Scanning Probe Microscopy and First Principles Studies

ANIKETA SHINDE,[a,b] JUEXIAN CAO,[b] RUQIAN WU,[b] AND REGINA RAGAN[a,*]
[a]Department of Materials Science and Chemical Engineering and [b]Department of Physics and Astronomy, University of California, Irvine, California 92697-4575, USA

(Received 2 February 2008 and in revised form 16 July 2008)

Abstract. We performed systematic experimental and computational studies to investigate the adsorption geometries of Y atoms on the Si(001) surface. This paves a way for understanding and eventually controlling the growth of rare earth disilicide wires on the Si(001) substrate that are promising for various applications. For a single Y atom, the interrow$_{dn}$ site was found to be at least 400 meV lower in energy than other possible binding sites. The emulated STM images are in good agreement with experimental results of Er on Si(001). The strong bias and coverage dependence indicates the need for theoretical guidance for the correct interpretation of experimental data. We elucidate the Y–Si binding mechanism and provide insights toward the onset of formation of hexagonal rare earth disilicide wires.

INTRODUCTION

Rare earth disilicides ($RESi_{2-x}$), in particular erbium disilicide ($ErSi_{2-x}$) and dysprosium disilicide ($DySi_{2-x}$), are of enormous interest due to their high conductivity and low Schottky barrier on *n-type* silicon.[1] Preinesberger et al. were the first to observe that growth of $DySi_{2-x}$ on Si(001) resulted in formation of nanowires (wires) along the two orthogonal Si[110] directions with a length-to-width aspect ratio up to 100.[2] Chen et al. later demonstrated that $ErSi_{2-x}$ on Si(001) adopts a similar growth morphology and proposed that the asymmetric strain between $RESi_{2-x}$ in the hexagonal aluminum diboride (AlB_2)-type crystal lattice and the Si(001) diamond cubic crystal lattice was the driving force for the development of one-dimensional structures.[3] Recent transmission electron microscopy analysis of $DySi_{2-x}$ wires on Si(001) confirmed that the wires adopt a hexagonal lattice with their length along the *a* axis and width along the *c* axis, as sketched in Fig. 1.[4,5] While wires form in two orthogonal directions on flat Si(001), Ragan and coworkers demonstrated that $ErSi_{2-x}$ and Sm_3Si_5 wires form parallel arrays along a single Si[110] direction, perpendicular to the Si dimer rows, when grown on vicinal Si substrates with a 2.5° miscut toward [110].[6] Shortly afterwards, Nogami and Liu also demonstrated growth of parallel arrays of $GdSi_{2-x}$ wires on vicinal Si(001).[7] Significantly, although $RESi_{2-x}$ wires have a highly reactive surface, nanostructures are able to remain structurally stable when submonolayer Pt is deposited on the surface.[8] High-density arrays of $RESi_{2-x}$ wires can therefore be used for selective aggregation of platinum[9] and gold[10] atoms on $RESi_{2-x}$ wire surfaces

*Author to whom correspondence should be addressed.
E-mail: rragan@uci.edu

DOI 10.1560/IJC.48.2.73

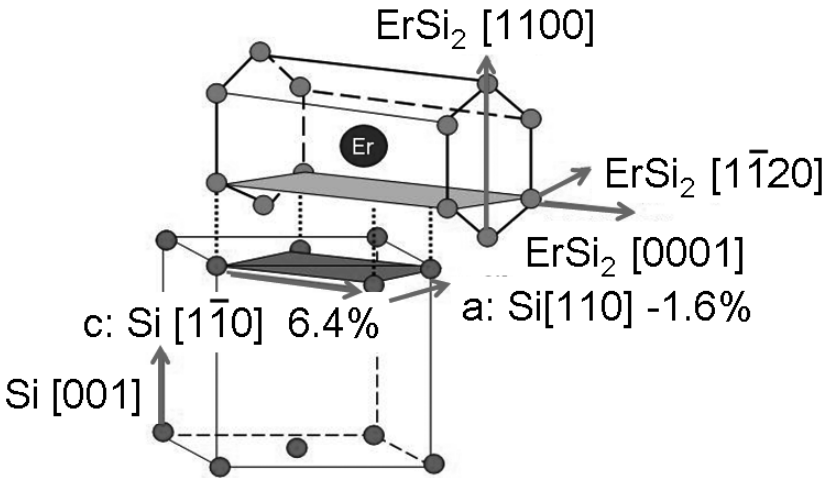

Fig. 1. Diagram indicating the geometrical mismatch of an $ErSi_2$ unit cell and Si(001) surface (in color online).

versus the silicon substrate. Combined with reactive ion etching, this process permits massive production of core–shell Pt/$RESi_{2-x}$ nanostructures with a diameter of less than 10 nm, a size distribution narrower than ±1 nm, and inter-particle spacing around 10 nm without lithography.[9] These monodisperse nanostructures may be exploited in many fields such as catalysis, sensing, and microelectronics.

To control the growth morphology and physical properties of $RESi_{2-x}$ nanostructures, it is crucial to understand the interaction between RE atoms and the Si substrate. Much of the previous work on $RESi_{2-x}$/Si(001) systems has involved scanning tunneling microscopy (STM) characterization of nanostructures and adsorption geometries of RE adatoms on Si(001), but the interpretation of STM images is often ambiguous. Very few theoretical studies have been performed on these systems with the modern density functional theory (DFT). The lack of clear understanding of these important systems motivated us to perform systematic density functional studies and compare them with experimental results. This study provides a basis for understanding the surface morphology of RE atoms on Si prior to wire nucleation and for correct interpretation of STM images in further investigations.

EXPERIMENTAL

Si(001) surfaces were prepared by annealing substrates at 650 °C overnight in an ultrahigh vacuum (UHV) system with a base pressure of 9×10^{-11} Torr. After the sample cooled to room temperature, the Si(001) substrate was heated to approximately 1200 °C for 5 s while keeping the chamber pressure below 5×10^{-10} Torr. After 5 s, the sample temperature was rapidly dropped to 900 °C, then slowly cooled to 600 °C, and held at 600 °C for 30 min before being allowed to cool to room temperature. The temperature was measured with an optical pyrometer with an emissivity setting of 0.7. STM images were acquired to confirm a 2 × 1 reconstructed Si(001) surface before deposition of RE metal. Er was evaporated from a molybdenum crucible onto 2 × 1 reconstructed Si(001) substrates heated to approximately 600 °C using an in situ Mantis mini E-beam evaporator. An Omicron variable temperature STM and atomic force microscope (AFM) were in a UHV chamber attached to the deposition system for analysis of structures without exposure to ambient conditions. All STM images were acquired at room temperature under constant current mode.

COMPUTATIONAL APPROACHES

First principles calculations were performed within the density functional framework using the generalized gradient approximation (GGA) for the exchange correlation energy functional (PW 91), as implemented in the Vienna ab initio Simulation package (VASP).[11] Ultra-soft pseudopotentials (US PP) were used to represent the electron interaction with ionic cores.[12] A plane-wave basis set with an energy cutoff of 350 eV was used. The Si(001) surface is modeled by periodically repeating slabs made up of 6 layers of Si(001) and 15 Å of vacuum. On the lateral plane, we adopted a (3 × 4) supercell to mimic the low adsorption environment. The 2 × 2 × 1 *k*-points were used to sample the Brillouin zone. The top 3 layers of Si along with the adatoms were allowed to relax, with a criterion that forces are lower than .01 eV/Å. The bottom 3 layers of Si were fixed, and dangling bonds were passivated with hydrogen.

To circumvent the problem dealing with the strongly localized 4*f* shell of rare earth pseudopotentials, we used yttrium to represent RE elements. Y is a trivalent

atom that does not have *f* valence electrons but has chemical and physical properties very similar to the RE elements.[13] For example, the atomic and electronic structures of YSi_2 monolayers on Si(111) were found to resemble $RESi_{2-x}$ thin films using low-energy electron diffraction and density functional calculations.[14, 15] Test calculations confirmed the adequacy of our model and parameters. For example, our calculations converged to the well-known Si dimer structure of clean Si(001) surfaces, as reported extensively in the literature.[16] The change of adsorption energies of a single Y adatom on a thicker Si(001) slab, 8- or 12-layers, was less than the thermal energy for RE deposition on Si at 600 °C (75 meV).

RESULTS AND DISCUSSION

Figure 2(a) is a typical STM image of $ErSi_{2-x}$ wires having an Er coverage of approximately 0.1 monolayer (ML) on a vicinal Si(001) surface with a 2.5° miscut toward [110]. A line profile taken from across the diagonal of Fig. 2(a) is shown in Fig. 2(b). From this line profile, the average wire width and the average distance between them are 3.2 nm and 10.2 nm, respectively. Analysis of line profiles from STM data from Fig. 2(a) yielded nanowire heights approximately 1–2 silicide layers high, where 1 silicide layer is .33 nm in the surface normal direction.[17, 18] A zoom-in STM image of a 30 nm × 30 nm region of a sample with Er coverage slightly less than 0.1 ML is shown in Fig. 2(c). Various periodicities, or surface reconstructions, can be seen on the Si(001) surface between $ErSi_{2-x}$ wires that result from various numbers of Er atoms in a group on the Si(001) surface. As a reference for lattice size and orientation, the bright features extending along the [110] direction are Si dimer rows. Although $[1\bar{1}0]$ and [110] are indistinguishable directions in the bulk, the symmetry is broken on the surface of a reconstructed Si(001) terrace due to dimer formation. In this paper, $[1\bar{1}0]$ refers to a direction perpendicular to dimer rows and [110] indicates the direction parallel to dimer rows on a terrace. The high-resolution STM image of Fig. 2(d) acquired for the occupied states shows that along $[1\bar{1}0]$ the periodicity of the small bright features in the metal reconstructed region is the same as that of the dimer rows, 2 × 3.84 Å, or 2 a_{Si}. The Si dimers at the lower left corner of Fig. 2(d), indicated by an arrow, provide a natural scale marker for a_{Si} along [110], where the zigzag pattern of the buckled dimer has a periodicity of 2 a_{Si}. It is interesting that the spacing between small dim features along [110] is also an integer value of a_{Si}, typically 2 or 3. We can therefore conclude that the Er atoms form commensurate structures along [110] on the Si(001) substrate. However, it is difficult to tell the location of metal atoms and the metal-induced surface reconstruction merely from the STM images.

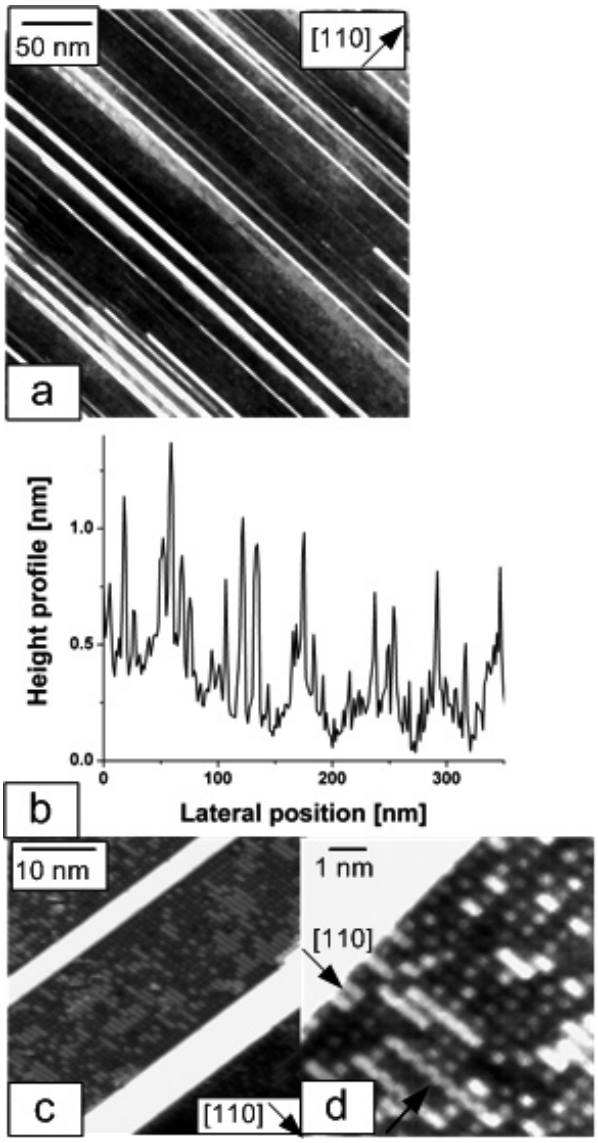

Fig. 2. STM images acquired with a feedback current of 100 pA of (a) 250 nm × 250 nm region $ErSi_{2-x}$ nanowires on a vicinal Si(001) substrate with a 2.5 degree miscut toward [110] at V_{bias} = –1.9V. The line profile across the diagonal is shown in (b). $ErSi_{2-x}$ nanowires on nominally flat Si(001) substrate of a (c) 30 nm × 30 nm region at V_{bias} = –1.9V and (d) 10 nm × 10 nm region at V_{bias} = –2.1V. The bright intensity in the upper left hand corner of the image in (c) results from a nanowire on the surface. The arrow in the lower left corner (d) points to buckled Si dimers on the surface (in color online).

To aid in interpreting STM images correctly, we performed density functional calculations for the preferred adsorption site of Y on the reconstructed Si(001) substrate, starting from geometries as shown in Fig. 3. As

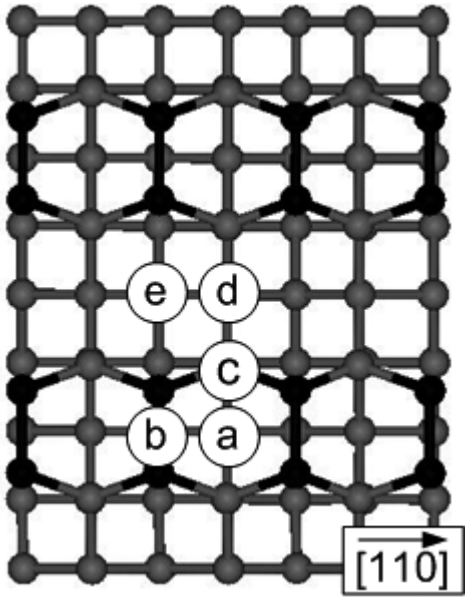

Fig. 3. Top view of possible binding sites for Y adatoms (white circles) on reconstructed Si (black circles) surface with four layers of bulk shown (gray circles): (a) cross row; (b) ondimer; (c) intrarow; (d) interrow$_{dn}$; (e) interrow$_{up}$.

a common practice in theoretical studies, the stability is characterized by adsorption energies, defined as

$$E_b = E[\text{Y Adatom}]–E[\text{Y atom}]–E[\text{Si(001)}]$$

Spin-polarized calculations were done to account for the nonzero magnetic moment of a single Y atom. As expected, the *p*(Si)– *d*(Y) hybridization quenches the magnetic moment of Y *d* electrons, as found in previous DFT calculations done by Szwacki and Yakobson.[19] From the values of E_b in Table 1, we found that site (d) interrow$_{dn}$, located between Si dimer rows, is the most stable place for Y, with adsorption energy as low as –7.008 eV. Particularly, a Y adatom initially placed on the (c) site shifts to the (d) site in the structural optimization procedure. This indicates that there is no potential energy barrier between these two sites and it is rather easy for Y to migrate to the (d) site. Note that the adsorption energy for Y on the (b) site, the bridge position over the Si dimer, is significantly higher than that of the ground state geometry. It is also important to mention that the presence of a

Table 1. Binding energies for sites a, b, d, and e, as shown in Fig. 1. The binding energy for c is not shown since the atom moved to position d in the relaxed structure

binding site	E_b [eV]
a	–5.668
b	–6.125
d	–7.008
e	–6.592

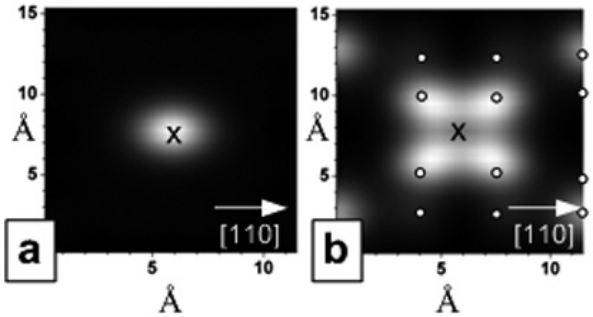

Fig. 4. Simulated STM image for 1 Y atom at site d with (a) V_{bias} = +2 V and (b) V_{bias} = –2 V. The Y position is indicated by an "×" and surface Si in dimer locations are indicated by small white circles.

single Y atom does not break surrounding Si dimers, as seen in the experimental data of Fig. 2(d), which shows the presence of metal atoms along with Si dimer rows.

For direct comparison to experimental data, we generated constant-current STM images within the Tersoff–Haman[20] scheme using wavefunctions of the density functional calculations. Figure 4 shows the simulated STM image of Y/Si(001) in a region of 15 Å × 11.5 Å for both the empty and occupied states. It is interesting to note that the simulated intensity on top of the Y atom switches with sample bias. While one bright protrusion on Y is found for the empty states (+2 V sample bias), four lobes are found on top of Si atoms for the occupied states (–2 V sample bias). A dark spot takes the position on top of Y in the image of occupied states. From the simulations one can conclude that the position of a Y atom does not necessarily overlap with a bright feature in the occupied states STM images, and, furthermore, there is no direct correspondence between the number of bright spots and number of adatoms. The shift in the position of bright features between empty and occupied states images is also observed in experiment, as shown in the STM data in Fig. 5. Figures 5(b) and 5(c) are acquired from the same location on the surface with a bias of +2.0 V in the backward scan and –2.1 V in the forward scan, respectively. The "×" marks the same location in images 5(b) and 5(c), presumably right on top of an Er adatom, as discussed above. The strong bias dependence of STM images may be a reason for different surface morphologies reported for Er[21] and Dy[22,23]. The occupied states image of Fig. 5(c) represents what has been reported as a c(4 × 2) reconstruction for Er on Si(001),[21] whereas the empty states image of Fig. 5(b) shows what appears to be a (4 × 8) reconstruction that has not been reported previously. It should be noted that STM images are not only bias dependant but coverage dependant as well, as discussed in previous work for Er and Dy induced reconstructions.[21,22]

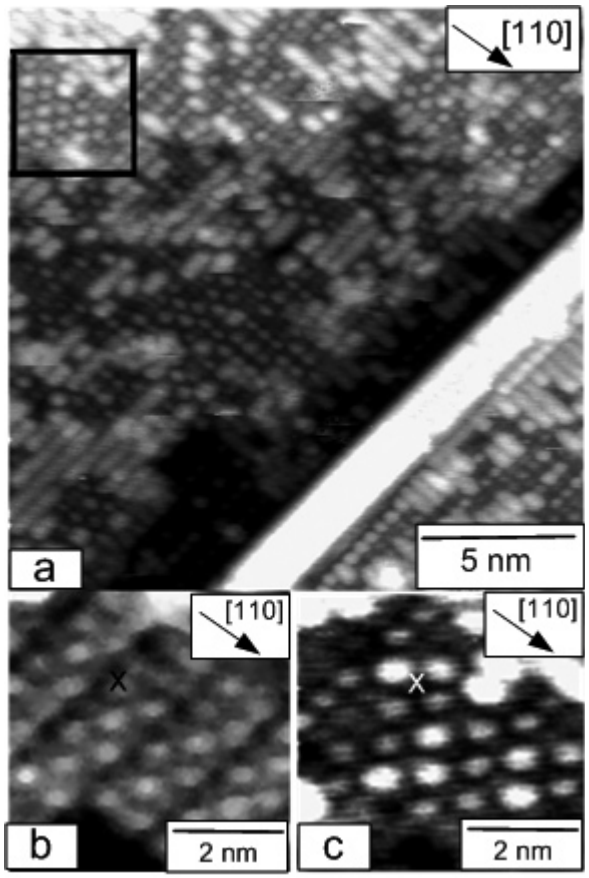

Fig. 5. (Color online.) STM images acquired with a feedback current of 100 pA of Er on nominally flat Si(001) substrate of (a) a 25 nm × 25-nm region at V_{bias} = –2.1V and (b) a 5 nm × 5-nm region at V_{bias} = +2.0 V that is highlighted by the black box in (a). The same highlighted 5 nm × 5 nm region in (b) acquired at (c) V_{bias} = –2.1 V (in color online).

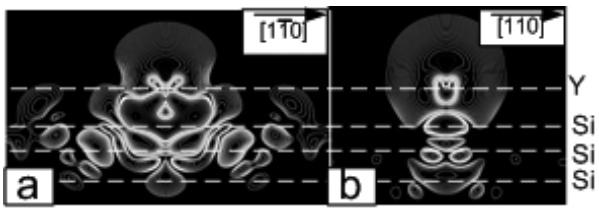

Fig. 6. Simulated charge density difference images for 1 Y atom at site (d) on Si(001) with the cross section along (a) [110] direction and (b) [1 $\bar{1}$ 0]. Blue represents charge depletion and pink represents charge accumulation. Contours start from ±0.001 e/Å^3 (yellow and green contour lines) where e is the electron charge, and change successively by a factor of $\sqrt{2}$ (in color online).

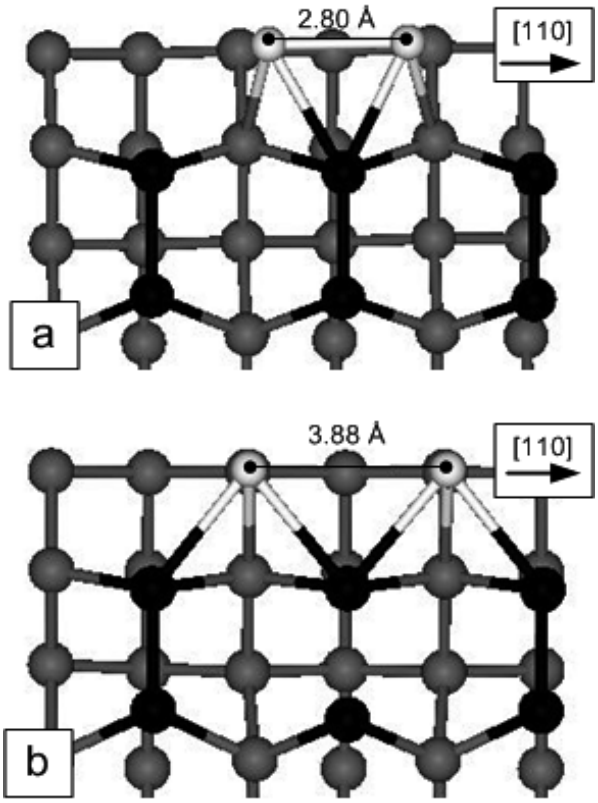

Fig. 7. Ball and stick model for (a) initial positions of two Y atoms arranged close enough for dimer formation on reconstructed Si(001) and (b) relaxed Y atom positions, showing that the Y atoms move apart.

To reveal the Y–Si bonding mechanism, we produced contours of charge density difference, $\rho_{Y/Si\ (001)} - \rho_{Si(001)} - \rho_Y$, as shown in Fig. 6(a) and 6(b). It is clear that charge leaves the Y atom (blue) and accumulates between Y and the subsurface Si atoms (pink). Y cations are therefore repulsive toward each other, and one expects that they spread rather uniformly on the Si(001) surface.

STM experiments done by Yang and coworkers at low coverage of Er on Si(001) measured (2 × 3) and c(4 × 2) reconstructions on surfaces. The data were interpreted as Er atoms forming dimers on Si(001),[21] while Liu and Nogami suggest that single Dy atoms form the (2 × 4) and (2 × 7) reconstruction.[22,23] In order to test whether it is energetically favorable for RE dimer formation on Si(001), we also explored various configurations with two Y atoms. As a result, two Y atoms take the adjacent (d) sites, and the separation closely matches the substrate periodicity, a_{Si}. No stable Y dimer was found from all the initial setups. As an example, the initial and relaxed atomic positions are shown in Figs. 7(a) and 7(b). From the relaxed image of Fig. 7(b), one observes that Y atoms tend to push each other apart due to the Coulomb repul-

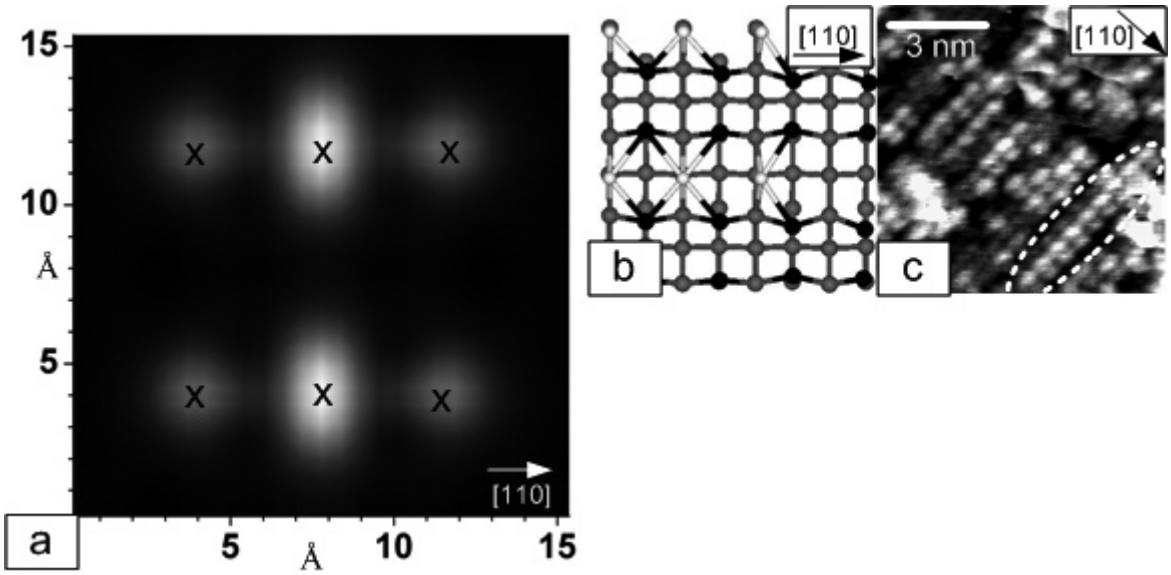

Fig. 8. (a) Simulated STM image at V_{bias} = +.7 V of 6 Y atoms on Si(001) with the atomic positions indicated by an "×", (b) ball and stick model of the simulated image of (a) showing the 6 Y (white circles) atoms at site d, surface Si that form dimers (black circles) and four Si layers underneath (gray circles). (c) (Color online) The experimental STM data were acquired with V_{bias} = +0.7 V and a tunneling current of 100 pA.

sion between the two positive ions. Clearly, our calculations deny formation of RE dimers on Si(001).

Finally, we also investigated stable geometries with high Y coverage. Six Y atoms were placed at site (d) on a (4 × 4) unit cell so as to allow complex local reconstructions. As shown in Fig. 8(b), Y forms commensurate chains along [1 $\bar{1}$ 0] and the presence of groups of Y atoms opens Si dimers nearby. The simulated STM image for empty states is shown in Fig. 8(a), under a bias of +0.7 V. The periodicity and the elliptical shape of the center feature in the simulated image are also observed in experimental STM images under the same bias in Fig. 8(c). The dashed oval at the bottom right corner highlights a region that has three protrusions along the [110] direction. Because of the difference in their environment, the brightness on top of the central Y atom is different from the edge Y atoms in both Figs. 8(a) and 8(c). This alternating intensity has been observed by Liu and Nogami for Dy on Si(001) at a bias of +0.46 V.[22] It was hypothesized that this may be due to a buckling of Dy atoms. However our DFT calculations did not show any meaningful buckling of Y atoms. The alternating intensity in the empty states image is associated with the change of wavefunction rather than topography.

The preferential binding site (d) found in our calculations is a natural starting point for the formation of a disilicide crystal in the AlB_2 type crystal structure. In this hexagonal lattice, a RE atom sits between two planes of Si, each with 6 Si atoms forming a hexagon, as seen in Fig. 1. A RE adatom at site (d) interacts with four surface Si atoms and potentially two subsurface Si atoms, as seen in Fig. 3 of the relaxed configuration for 1 Y atom at site (d). For several Y atoms along [1 $\bar{1}$ 0], the Si dimers nearby are opened. It is ready to form the hexagonal structure with *a* along [1 $\bar{1}$ 0] and *c* along [110] if additional Si atoms are provided.

CONCLUSIONS

Synergistic ab initio calculations and STM measurements performed for Y on Si(001) revealed the mechanism of adsorbate–substrate interaction and the precursor state for the formation of $RESi_{2-x}$ wires. In addition, calculations revealed that formation of RE dimers or buckling structures on Si(001) is unlikely. Stable positions for Y on Si(001) surface are the interrow$_{dn}$ sites (d), which are compatible with the AlB_2 hexagonal structure of $RESi_{2-x}$ wires with additional Si atoms. We pointed out that one needs to be very cautious when interpreting STM images because of their strong bias and coverage dependence. This study provides a basis for further morphological studies of $RESi_{2-x}$ wires on Si(001) and adsorption of noble metal atoms on the surfaces of these wires.

Acknowledgments. Acknowledgment is made to the donors of the American Chemical Society Petroleum Research Fund for partial support of this research and National Science Foundation CBET-0731349 & CBET-0642217. RW also acknowledg-

es support from DOE-BES DE-FG02-04ER15611. AS would like to acknowledge Dr. C. Jo and S. Lee for useful discussions and the 2006 CALIT^2 Graduate Fellowship for support. Calculations were performed on NERSC supercomputers.

REFERENCES AND NOTES

(1) Tu, K.N.; Thompson, R.D.; Tsaur, B.Y. *Appl. Phys. Lett.* **1981**, *38*, 626–628.
(2) Preinesberger, C.; Vandre, S.; Kalka, T.; Dahne-Prietsch, M. *J. Phys. D: Appl. Phys.* **1998**, *31*, L43–L45.
(3) Chen, Y.; Ohlberg, D.A.A.; Medeiros-Ribeiro, G.; Chang, Y.A.; Williams, R.S. *Appl. Phys. Lett.* **2000**, *76*, 4004–4006.
(4) Ye, G.F.; Crimp, M.A.; Nogami, J. *Phys. Rev. B.* **2006**, *74*.
(5) Ye, G.F.; Nogami, J.; Crimp, M.A. *Thin Solid Films* **2006**, *497*, 48–52.
(6) Ragan, R.; Chen, Y.; Ohlberg, D.A.A.; Medeiros-Ribeiro, G.; Williams, R.S. *J. Cryst. Growth* **2003**, *251*, 657–661.
(7) Liu, B.Z.; Nogami, J. *Nanotechnology* **2003**, *14*, 873–877.
(8) Ragan, R.; Kim, S.; Li, X.; Williams, R.S. *Appl. Phys. A* **2005**, *80*, 1339–1342.
(9) You, J.P.; Choi, J.H.; Kim, S.; Li, X.M.; Williams, R.S.; Ragan, R. *Nano Lett.* **2006**, *6*, 1858–1862.
(10) Ragan, R.; Kim, S.; Chen, Y.; Li, X.; Williams, R.S. *Proc. SPIE* **2004**, *5593*, 167–172.
(11) Kresse, G.; Furthmuller, J. *Phys. Rev. B.* **1996**, *54*, 11169–11186.
(12) Kresse, G.; Joubert, D. *Phys. Rev. B.* **1999**, *59*, 1758–1775.
(13) Magaud, L.; Veuillen, J.Y.; Lollman, D.; Tan, T.A.N.; Papaconstantopoulos, D.A.; Mehl, M.J. *Phys. Rev. B.* **1992**, *46*, 1299–1304.
(14) Rogero, C.; Koitzsch, C.; Gonzalez, M.E.; Aebi, P.; Cerda, J.; Martin-Gago, J.A. *Phys. Rev. B.* **2004**, *69*.
(15) Rogero, C.; Polop, C.; Magaud, L.; Sacedon, J.L.; de Andres, P.L.; Martin-Gago, J.A. *Phys. Rev. B.* **2002**, *66*.
(16) Kubby, J.A.; Boland, J.J. *Surf. Sci. Rep.* **1996**, *26*, 61–204.
(17) Liu, B.Z.; Nogami, J. *J. Appl. Phys.* **2003**, *93*, 593–599.
(18) He, Z.A.; Smith, D.J.; Bennett, P.A. *Phys. Rev. B.* **2004**, *70*.
(19) Szwacki, N.G.; Yakobson, B.I. *Phys. Rev. B.* **2007**, *75*.
(20) Tersoff, J.; Hamann, D.R. *Phys. Rev. B.* **1985**, *31*, 805–813.
(21) Yang, J.S.; Cai, Q.; Wang, X.D.; Koch, R. *Surf. Sci.* **2003**, *526*, 291–296.
(22) Liu, B.Z.; Nogami, J. *Surf. Sci.* **2001**, *488*, 399–405.
(23) Liu, B.Z.; Nogami, J. *Surf. Sci.* **2003**, *540*, 136–144.